

Three-dimensional structure of a viral genome-delivery portal vertex

Adam S. Olia¹, Peter E. Prevelige Jr.², John E. Johnson³ and Gino Cingolani⁴ †

¹ *Department of Biological Sciences, Purdue University, 240 Martin Jischke Boulevard, West Lafayette, Indiana 47907, USA.*

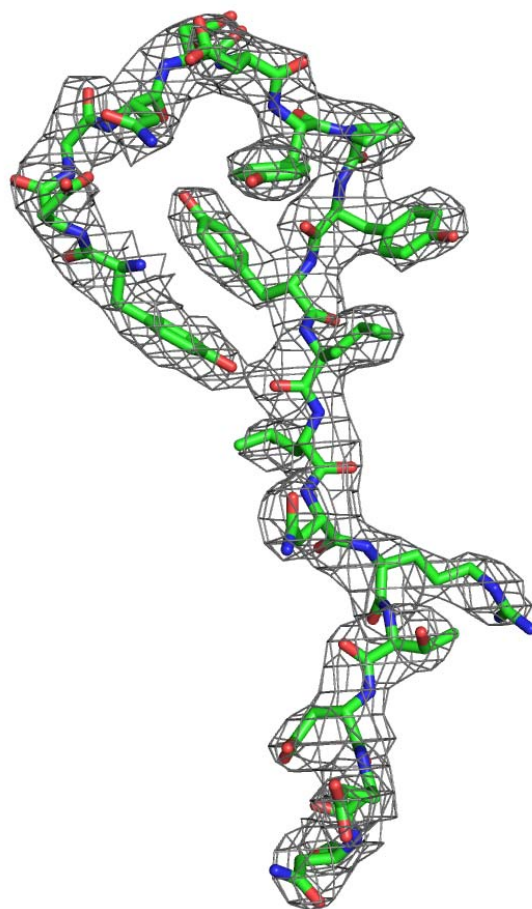
² *Department of Microbiology, University of Alabama at Birmingham, Birmingham, Alabama 35294, USA.*

³ *Department of Molecular Biology, The Scripps Research Institute, 10550 North Torrey Pines Road, La Jolla, California 92037, USA.*

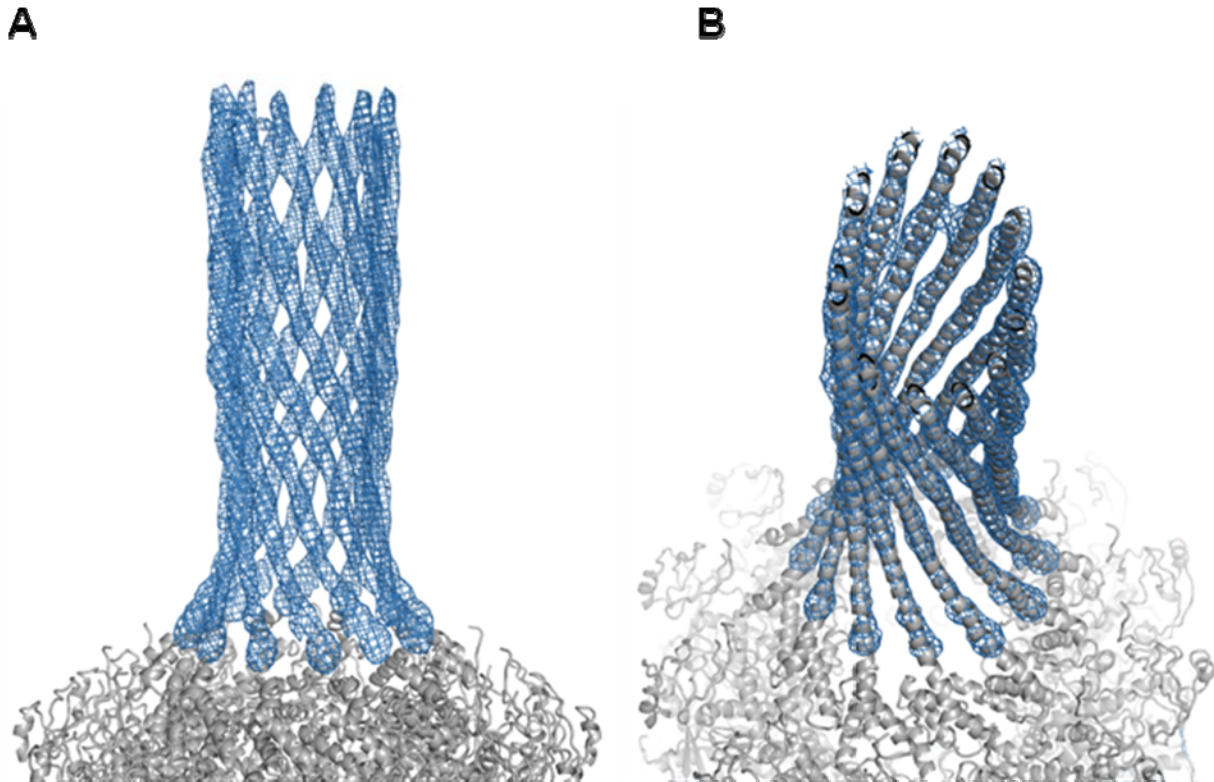
⁴ *Department of Biochemistry and Molecular Biology, Thomas Jefferson University, 233 South 10th Street, Philadelphia, Pennsylvania 19107, USA.*

† Corresponding author

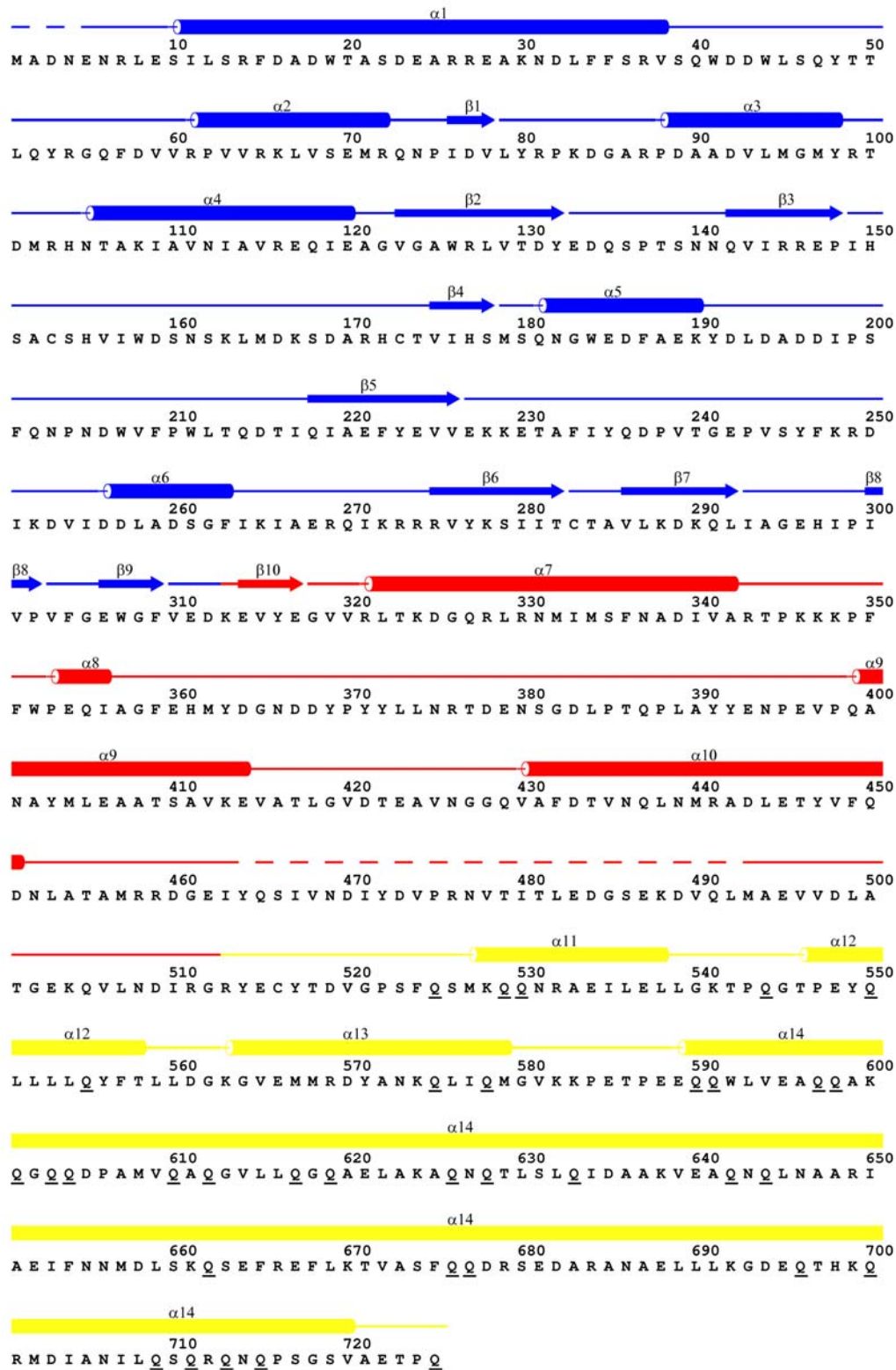
Tel.: (215) 503 4573; FAX: (215) 464 4595; E-mail: gino.cingolani@jefferson.edu



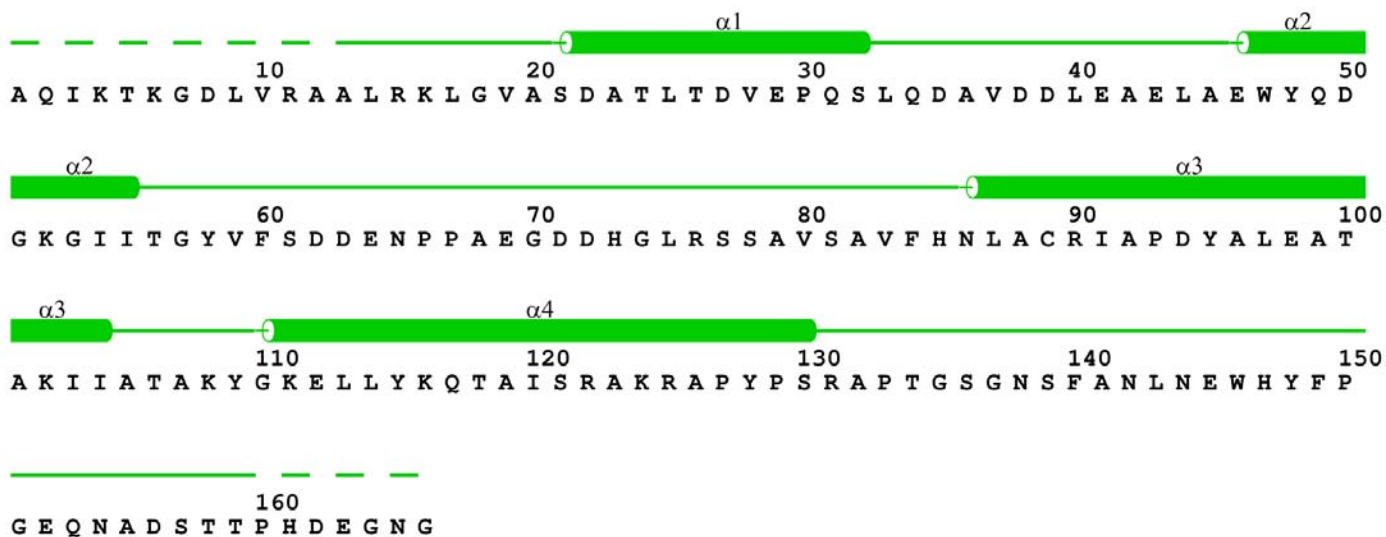
Supplementary Figure 1: Representative 24-fold Averaged Electron Density. The σ_A -weighted, 24-fold averaged 2Fo–Fc map computed to 3.25 Å resolution around a portion of the final model of portal protein core–gp4 (Tyr363–Asn380), which is represented as sticks. The density is displayed as gray mesh at 2.8σ above background. The illustration was generated using PyMol¹.



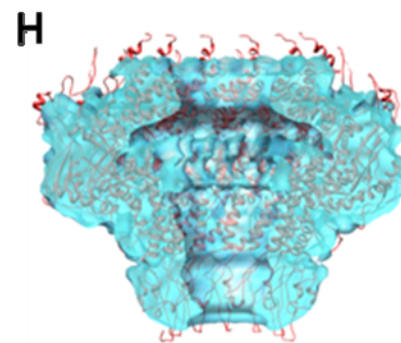
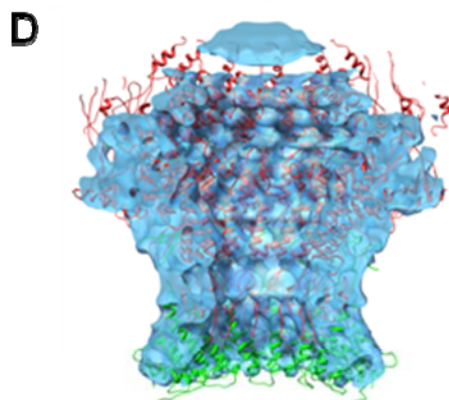
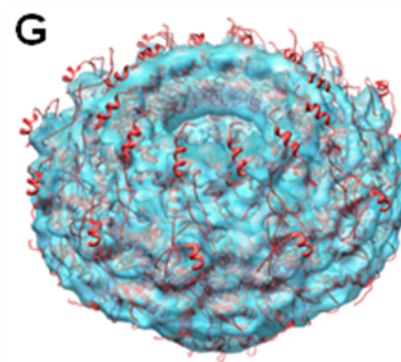
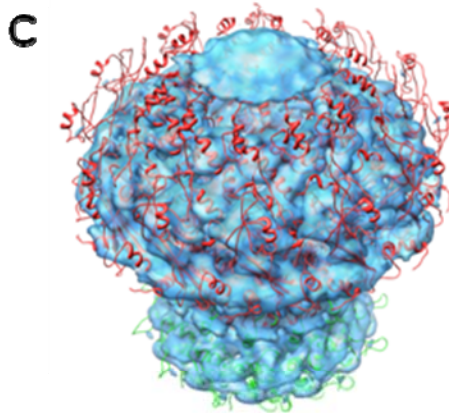
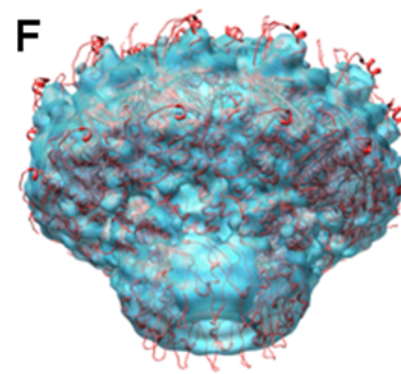
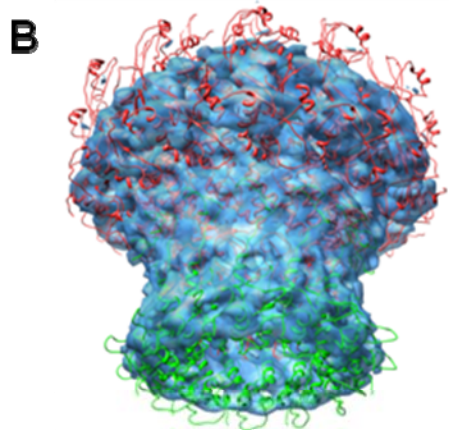
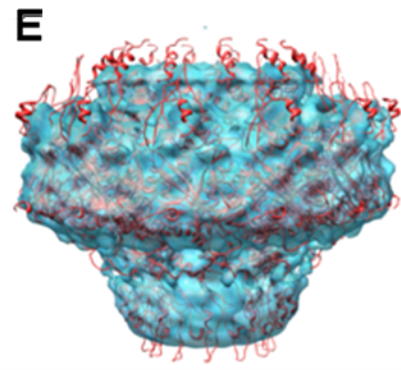
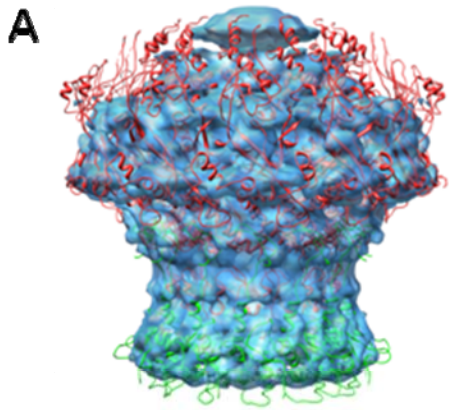
Supplementary Figure 2: Representative electron density map for full length portal protein. (A) The 7.5 Å σ_A -weighted 12-fold averaged Fo–Fc difference electron density map computed using phases from the portal protein core (res. 1–602) and structure factor amplitudes from the full length portal protein (res. 1–725) is displayed around the helical barrel of the final full length portal protein model. (B) The barrel is tilted $\sim 45^\circ$ as compared to panel (A) and the final refined model (in ribbon) is superimposed to the density. In both panels, the difference electron density map is displayed at 2.5σ contour level above background. The illustration was generated using PyMol¹.



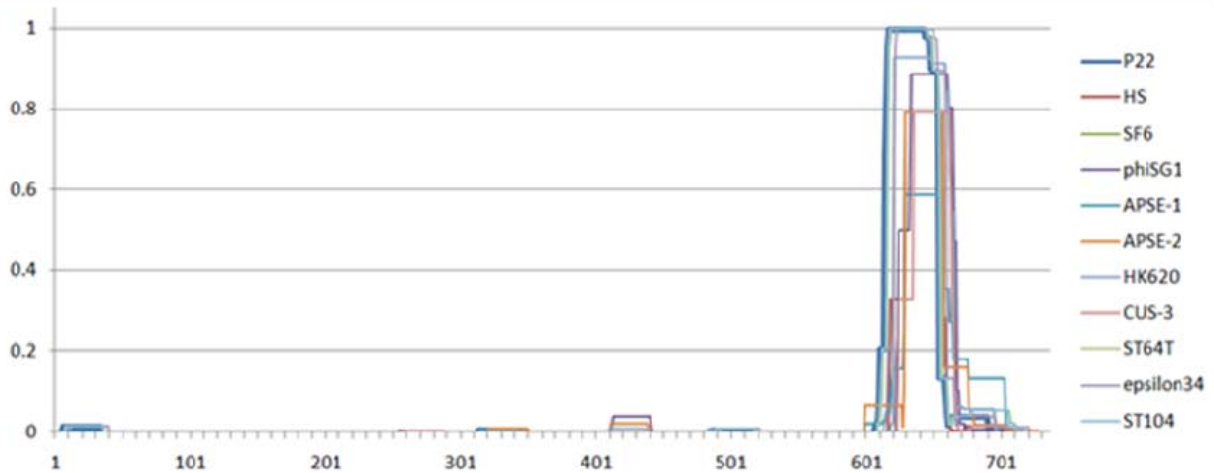
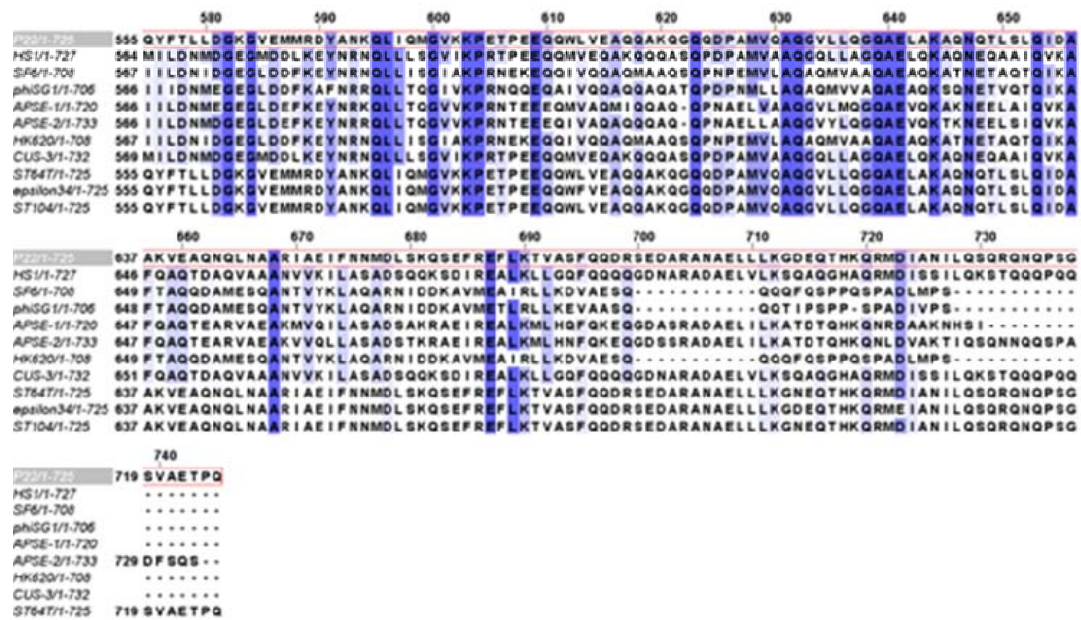
Supplementary Figure 3: Secondary structure and amino acid sequence of the P22 portal protein. The sequence is color-coded as in figure 2 to highlight the domain I, II and III, in blue, red and yellow, respectively. Gln residues in the barrel domain are underlined.



Supplementary Figure 4: Secondary structure and amino acid sequence of the middle ring factor gp4.



Supplementary Figure 5: Fitting of P22 portal protein and gp4 X-ray models into the cryo-EM reconstructions of the portal–gp4 complex (EMD-1482) and portal protein core (EMD-1483) determined by Zheng *et al.*². Panels A–D and E–H show the fitting of X-ray models inside cryo-EM reconstructions of the portal protein core–gp4 complex and free portal protein core determined by Zheng *et al.*², respectively. For each fitting, four views are presented: A and E show a side view; B and F a bottom-tilted view; C and G a top-tilted view; D and H show a section view. In all cases, the fitting between X-ray model and cryo-EM density is very poor. The ‘dome’ domain presented in the cryo-EM structure of the portal–gp4 complex does not exist neither in the X-ray model of portal protein core bound to gp4, nor in the cryo-EM of P22 mature virion³ (**Fig. 2** of this paper). This density likely represents an artifact of the cryo-EM reconstruction determined by Zheng *et al.*². Moreover, the twelve spokes of portal protein and the twelve gp4 equivalents bound to portal are significantly flattened in the cryo-EM reconstruction, as compared to the X-ray model, which fits perfectly into the P22 mature virion reconstruction³ (**Fig. 2**). Finally, the conformational changes in the DNA-pumping channel as a result of gp4 binding described by Zheng *et al.*² are completely disproved by the X-ray structures presented in this paper. In perfect agreement with the asymmetric cryo-EM reconstruction of mature P22 virion³ and the cryo-EM structure of the isolated P22 tail⁴ no significant conformational changes occur in P22 portal protein upon gp4 binding. Thus, the reconstruction by Zheng *et al.*² and the relative conclusions drawn by these authors concerning the dome domain and the conformational changes in the portal protein DNA-channel are likely incorrect.

A**B**

Supplementary Figure 6: A conserved coiled-coil motif in the C-terminus of Podoviridae portal protein. (A) Probability of coiled coil of several members of the Podoviridae family as determined by the software COILS⁵. Each shows an extremely high probability of a coiled coil between residues 600–650. Of note, the P22 portal (in dark blue), shows the same drop-off in coiled coil probability after residue 650, even though the structure clearly shows a continuous coiled coil extending to residue 720. (B) Sequence alignment of the barrel domain in several phages of the Podoviridae family obtained using the program ClustalW⁶. Highlighted in dark blue are identical residues conserved across all phages. In light blue are partially conserved residues.

Supplementary Table I: data collection, phasing and refinement statistics

	Portal Protein Core:gp4 complex			Full Length Portal
	L-P21	S-P21	L-P1	FL-Portal
Crystal Form	L-P21	S-P21	L-P1	FL-Portal
Beam-line	CHESS, A1	NSLS, X6A	NSLS, X6A	APS, BM14C
Spacegroup	P2 ₁	P2 ₁	P1	I4
Unit Cell (Å)	a = 170.1 b = 253.2 c = 281.8	a = 168.4 b = 254.9 c = 169.3	a = 167.8 b = 168.8 c = 256.3	a = 408.9 b = 408.9 c = 260.0
Angles (°)	α = 90.0 β = 90.7 γ = 90.0	α = 90.0 β = 118.2 γ = 90.0	α = 80.9 β = 89.7 γ = 59.1	α = 90.0 β = 90.0 γ = 90.0
Resolution (Å)	100 - 3.25 (3.37 - 3.25)	50 - 4.0 (4.14 - 4.0)	50 - 3.7 (3.83 - 3.7)	60 - 7.5 (7.67 - 7.5)
Reflections (total/unique)	1,005,613/ 350,168	477,281/ 110,191	294,573/ 168,971	97,006/ 27,188
Completeness (%)	92.2 (73.6)	98.9 (96.0)	89.2 (78.9)	99.5 (99.7)
R _{sym} ^a (%)	14.9 (57.3)	13.2 (47.4)	10.9 (47.4)	9.5 (77.7)
<I> / <σ _I >	8.7 (1.6)	13.1 (2.8)	8.4 (2.1)	12.7 (2.2)
Redundancy	2.9 (2.2)	4.6 (3.9)	1.7 (1.5)	3.6 (3.5)
B-factor from Wilson plot (Å ²)	84.0	106.0	85.3	236.6
Portal protomers in AU ^b	24	12	24	12
Refinement Statistics				
Resolution Used (Å)	20-3.25			60-7.5
Number of Reflections	304,497			25,572
Number of atoms	135,312			61,848
# of chains in AU ^b	48			12
# of residues in AU ^b	17,160			8,304
# of water molecules	528			0
R _{factor} / R _{free} ^c (%)	22.2 / 23.7			18.6 / 26.3
RMSD _{Bond} (Å)	0.006			0.014
RMSD _{Angles} (°)	0.97			1.1
Ramachandran Plot				
Most Favored (%)	73.9			74.9
Additionally Allowed (%)	21.7			20.8
Generously Allowed (%)	4.4			4.3
Disallowed (%)	0.0			0.0

Table S1. The numbers in parenthesis refer to the statistics for the highest resolution shell.
^a $R_{sym} = \sum_{i,h} |I(i,h) - \langle I(h) \rangle| / \sum_{i,h} |I(i,h)|$ where $I(i,h)$ and $\langle I(h) \rangle$ are the i^{th} and the mean measurement of the intensity of reflection h .

^b AU indicates the crystallographic asymmetric unit.

^c The R_{free} value was calculated using ~2,500 reflections selected in thin resolution shells.

Supplementary References

1. DeLano, W.L. www.pymol.org (2002).
2. Zheng, H. et al. A conformational switch in bacteriophage p22 portal protein primes genome injection. *Mol Cell* **29**, 376-83 (2008).
3. Lander, G.C. et al. The Structure of an Infectious p22 Virion Shows the Signal for Headful DNA Packaging. *Science* (2006).
4. Lander, G.C. et al. The P22 tail machine at subnanometer resolution reveals the architecture of an infection conduit. *Structure* **17**, 789-99 (2009).
5. Lupas, A. Prediction and analysis of coiled-coil structures. *Methods Enzymol* **266**, 513-25 (1996).
6. Przybylski, D. & Rost, B. Alignments grow, secondary structure prediction improves. *Proteins* **46**, 197-205 (2002).